Environ Earth Sci
DOI 10.1007/s12665-012-1591-5

ORIGINAL ARTICLE

Delineation of groundwater salinization in a coastal aquifer, Bousheher, South of Iran

Z. Mohammadi · M. Zare · B. Sharifzade

Received: 24 June 2011 / Accepted: 2 February 2012

Abstract The geochemical processes controlling chemical composition of groundwater are studied using hydrochemical and isotopic data in Abdan-Dayer coastal plain, south of Iran. The salinity of groundwater in the coastal plain ranges from 1,000, a fresh end-member, to more than 50,000 μS cm^{-1}, a saline end-member. Groundwater salinity increases from the recharge area toward areas with a shallow water table close to the Persian Gulf coast due to direct evaporation and sea water intrusion as confirmed by mixing binary diagrams, stable isotope content, and Br^{-}/Cl^{-} ratio. Groundwater flow pattern in the study area has been modified due to over-pumping of groundwater in recent years which resulted in further saline water migration toward fresh water and their mixing. The maximum mixing ratio is estimated about 15% in different parts of the study area according to chloride concentration.

Keywords Hydrochemistry · Mixing · Coastal aquifer · Salinity · Iran

Introduction

Coastal aquifers are the subsurface equivalents of coastal areas where continental fresh groundwater and seawater meet (Post 2005). Over-pumping of groundwater in coastal areas to meet the growing population demand for fresh water increases the effect of salinization processes. Furthermore, coastal areas in the arid and semi-arid conditions have higher vulnerability to salinization. Most of the coastal aquifers in Iran are situated along the northern edge of Persian Gulf characterized by arid and semi-arid climate conditions. These aquifer systems mostly show an unbalanced water budget. In addition, over-pumping in these coastal aquifers has resulted in groundwater quality deterioration. Growing demand for fresh water in coastal areas and the lack of resources other than groundwater in these areas make the coastal aquifers management a complicated task, due to processes affecting the groundwater quality and quantity.

Variation of chemical contents of groundwater in a coastal aquifer is investigated in this study. The chemical contents of water results from three factors: (1) the type of rock, (2) the chemical condition of water, and (3) the flow condition (Backalowicz 1994). As a result of these factors numerous chemical reactions produce chemical constituents in groundwater measured as groundwater quality or salinity (Hem 1985; Richter and Kreitler 1993; Drever 1982; Appelo and Postma 2005). Generally, salinization of groundwater may result from numerous processes such as intrusion of sea water, migration of saline water, evaporation, dissolution of minerals, mixing and pollution resulting from industrial, municipal, and agricultural activities (Vengosh and Rosenthal 1994; Petals and Diamantis 1999; Zammouri et al. 2007; Kouzana et al. 2009).

This study attempts to investigate the main processes controlling the groundwater hydrochemistry in Abdan-Dayer coastal plain, in South of Iran. Degrading of groundwater due to increase of salinity in the study area causes some problems for farmers. The study area is of particular importance as an active agricultural zone in Bousheher Province, South of Iran (Fig. 1). The results will provide essential guidelines for an optimum management of groundwater protection and pumping in the study area.

Z. Mohammadi (✉) · M. Zare · B. Sharifzade
Department of Earth Sciences, Shiraz University, Shiraz, Iran
e-mail: zmohamad@shirazu.ac.ir

Published online: 15 February 2012

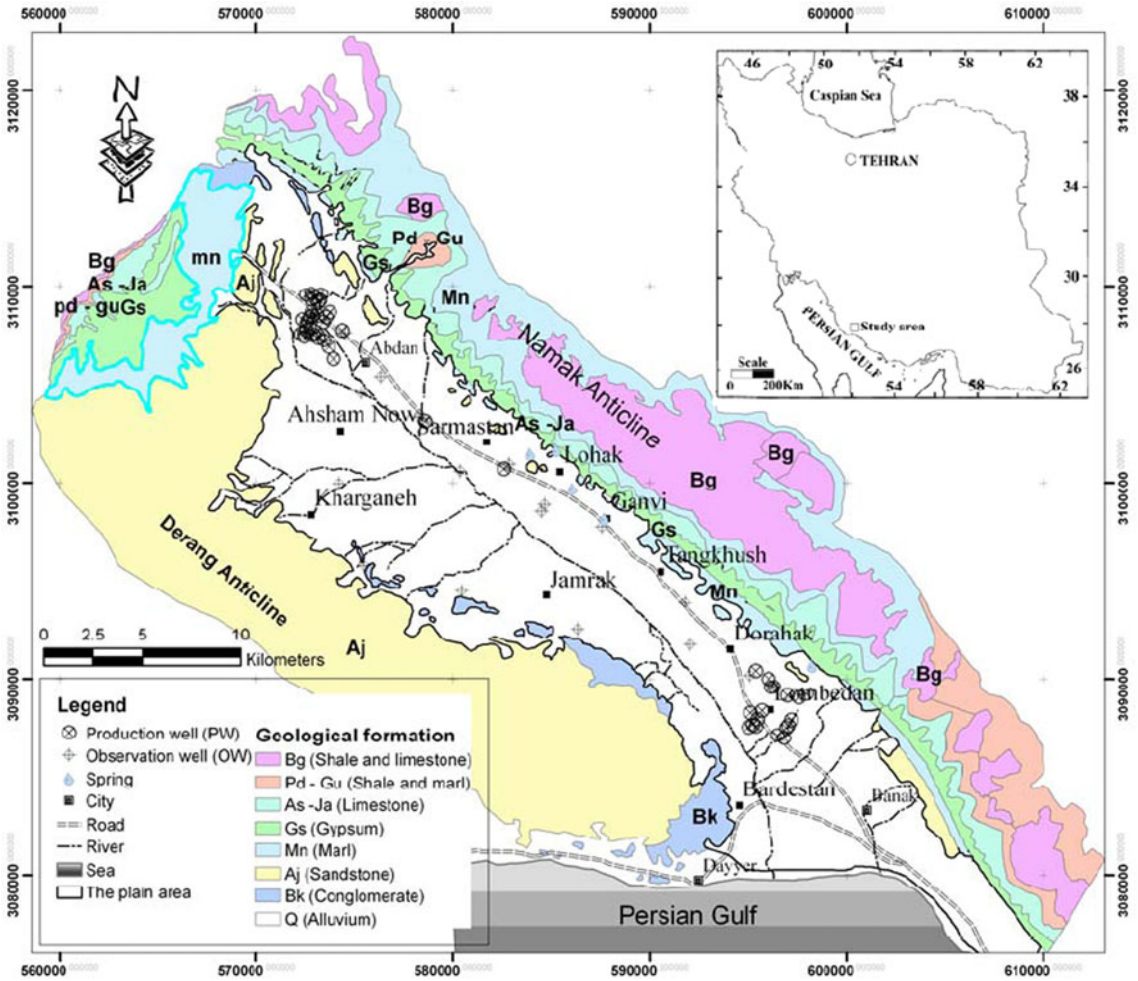

Fig. 1 Geological map of the study area including sampling points

Geological setting

Groundwater aquifer in the study area comprises quaternary alluvium which is surrounded by Namak Anticline (mainly limestone) to the north and north-west and Derang Anticline (mainly sandstone) to the south (Fig. 1). The southern part of the plain is in contact with Persian Gulf. Structurally, the plain is a part of the Zagros Mountainous Region. The Zagros Mountainous Region is one of the five major structural zones in Iran (Alavi 2004). The general geology and stratigraphy of the Zagros Region has been described in detail by Stocklin (1968) and Alavi (2004). The geological formations in decreasing age are Bangestan Group (Cretaceous), Pabdeh-Gurpi (Late Paleocene-Eocene), Asmari-Jahrom (Paleocene-middle Eocene), Gachsaran (early Miocene), Mishan (early to middle Miocene), Aghajari (late Miocene-Pliocene), Bakhtiari (upper Pliocene), and recent quaternary alluvium (Fig. 1). The Bangestan Group (Bg in Fig. 1) comprises bituminous shale and limestone, and outcrops in the core of the Namak Anticline. The Pabdeh-Gourpi (Pd-Gu in Fig. 1) Formation contains calcareous shale and gray marl and acts as a hydrogeological barrier. The Asmari-Jahrom (As-Ja in Fig. 1) and Gachsaran (Gs in Fig. 1) formations are the most important geological formations in the study area. The limestone terrain of the Asmari-Jahrom formation has a known potential for groundwater storage. The Gachsaran Formation comprises marl, gypsum, anhydrite, and salt where outcrops in the northern parts of the studied plain. The Mishan (Mn in Fig. 1), Aghajari (Aj in Fig. 1), and Bakhtiari (Bk in Fig. 1) formations mainly contain marl, sandstone, and conglomerate, respectively. The Namak anticline mainly comprises limestone layers of Asmari-Jahrom Formation and Bangestan Group while sandstone layers of the Aghajari Formation outcrops in the Derang Anticline.

The distribution and spatial variation of alluvial sediments (Q in Fig. 1) in the study area are investigated based on the geophysical studies and geological logging through 3 exploration and 17 observation wells (Bousheher Water

Authority 2005; Sharifzade 2009). The exploration studies defined an alluvial aquifer 100-m thick. A coarse sediment cover of up to 35 m thickness is laid on the upper parts of the aquifer. Generally, the sediments have coarse-sand size close to mountains, especially in northern margin of the plain changing to finer size in deeper and middle parts of the plain. The Bakhtiari Formation is the bed rock of alluvial aquifer in a syncline form.

Hydrogeological setting

Abdan-Dayer plain with an area of 370 km^2 behaves as a single unconfined aquifer. The Average transmissivity of this unconfined aquifer is 2,500 m^2 day^{-1} (Bousheher Water Authority 2000) and hydraulic gradient ranges from 0.0015 to 0.0038. Topographical surface dip is gentle toward south (Persian Gulf coast) with a slope of about 1–2%. Water table elevation ranges from 10 to −3 m relative to sea level, suggesting a hydraulic potential for sea water intrusion. However, it lowered about 10 m during 1999–2009 (Sharifzade 2009). Because of over-pumping in two parts (i.e., well fields) of the study area, namely Abdan and Lombedan villages (Fig. 1), groundwater level drawdown in these two locations is relatively high compared with other parts of the plain. Depth to groundwater table varies from <5 m in southern margin close to the Persian Gulf coast to more than 30 m in the northern-west margin of the plain. The regional groundwater flow in the studied aquifer is unusual and does not mimic the surface topography due to excess pumping through production wells which are concentrated in two well fields in the study area (Fig. 2). The regional groundwater flow in left part of the studied plain is from the southern margin to the north and north-west, based on potentiometric map (Fig. 2). The groundwater also has potential to flows from the sea coast to the aquifer. The Asmari-Jahrom limestone formations of Namak Anticline (Fig. 1) could recharge the aquifer through the northern boundary (Bousheher Water Authority 2000).

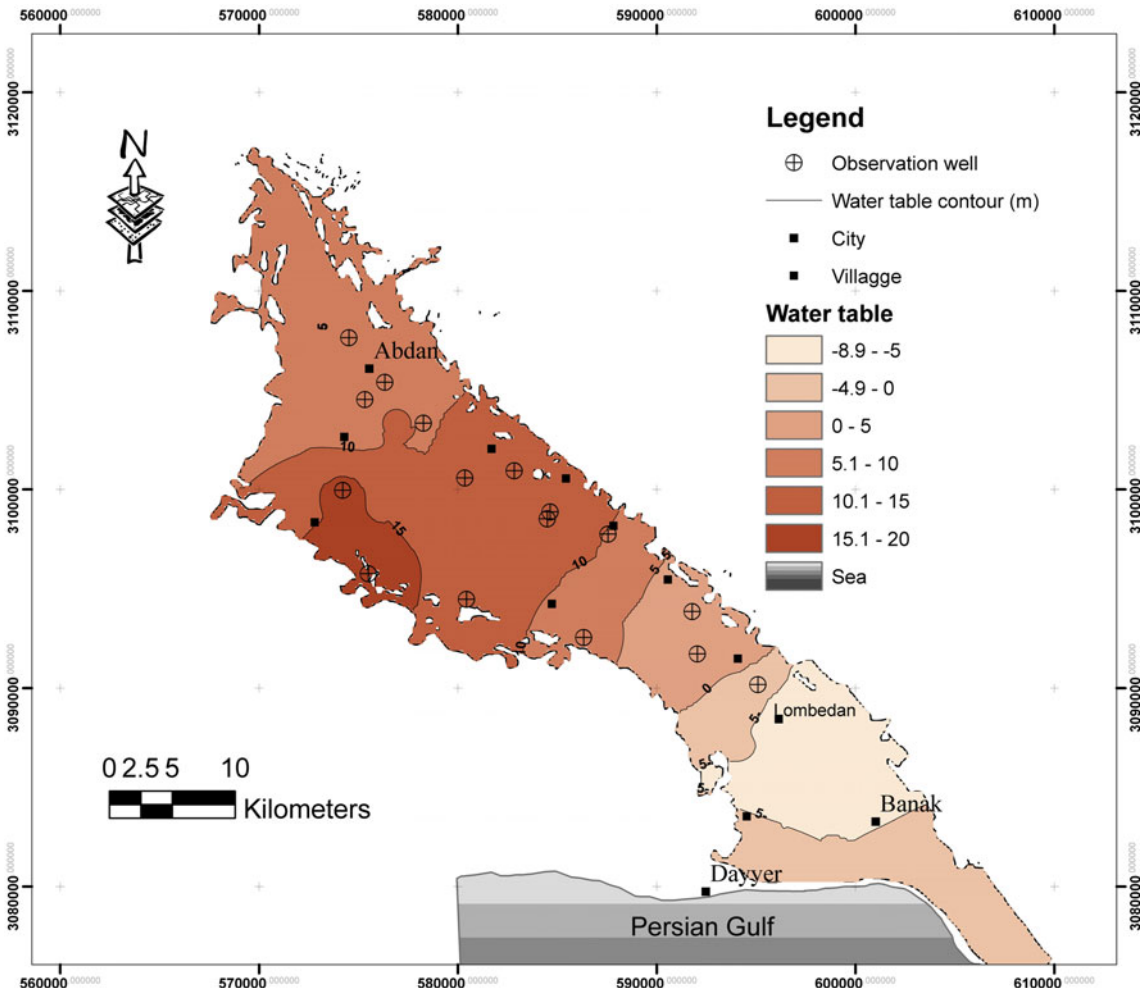

Fig. 2 Isopotential map in the study area (Oct. 2008)

Sampling and analysis

Sampling sites include two types of well: observation wells (denoted as OW in Fig. 1 and Table 1) and production wells (denoted as PW in Fig. 1 and Table 1). Samples for major ion analysis were collected from 16 observation wells, 53 productions wells, and 5 springs. Sea water samples were also collected on October 2008. Samples were tightly closed in 150 ml bottle after sampling. Water temperature, pH, and electrical conductivity (EC) were measured in the field by portable ELE instruments and major ions of water samples (Na^+, K^+, Ca^{2+}, Mg^{2+}, Cl^-, HCO_3^-, CO_3^{2-}, SO_4^{2-} and NO_3^-) were analyzed at laboratory. Calcium and Magnesium were measured by titration with EDTA, sodium and potassium were determined by flame photometry, chloride and sulfate were determined by turbidimetric methods, and bicarbonate was determined by titration with HCl. The quality of the analyses was evaluated using the ion balance (*IB*) equation as below:

$$IB = \left\{ \frac{|(\text{sum of cations} - \text{sum of anions})|}{(\text{sum of cations} + \text{sum of anions})} \right\} \times 100 \qquad (1)$$

where cations and anions are expressed in meq/l. All analyses were subjected to a less than 5% error (Table 1). The Br concentration was measured in 14 samples by ICP-MS method (Table 1) and 19 representative samples were collected for stable isotope analysis ($\delta^{18}O$ and $\delta^{2}H$). The isotope analyses were reported in ‰ versus Vienna standard mean ocean water (VSMOW) shown in Table 1.

Geochemical properties and salinization processes are interpreted as a result of using conventional graphical and Arithmetic methods such as Piper diagram, composite diagram, mixing estimations, and ionic deviation. The PHREEQC code (Parkhurst and Appelo 1999) was used to perform speciation and saturation index calculations (e.g., saturation state with respect to calcite, dolomite, gypsum, and halite).

Results and discussion

Chemical composition of groundwater

Results of hydrochemical and isotopic analyses are reported in Table 1. Groundwater temperature ranges from 20 to 24°C which is 6–10°C lower than ambient air temperature. All water samples measured in the field exhibited a pH range from 7.1 to 8.8. Values from wells are slightly alkaline >8. Water samples show a wide range of variation in EC values (from 1,000 to 50,000 μS cm^{-1}) as well as chloride concentration (from 63 to 21,000 mg l^{-1}). Most of the water samples could be considered as intermediate state of two end-members based on the chloride content as well as EC value including: fresh ($Cl < 300$ mg/l) and saline end-member ($Cl > 1{,}800$ mg/l). The fresh water samples are attributed to north and north-west margin of the plain. The saline groundwater samples are located in the southern and central parts as well as close to the coastal areas. Other samples are approximately distributed between these end-members.

Two end-members for the chemical facies are evident through plotting of the Piper diagram: Na–Cl and Ca–Mg–SO_4 facies (Fig. 3). However, some of samples are distributed between them. The spatial distribution of Ca–Mg–SO_4 facies in the study area, mainly fresh water samples, matches with the outcrops of Gachsaran Formation containing gypsum and anhydrite minerals. On the other hand, samples of Na–Cl facies correlate with the shallow groundwater and the areas close to the sea coast.

Saturation index with respect to Calcite (SIC), Dolomite (SID), Gypsum (SIG), and Halite (SIH) range from 0.3 to 1.4, 0.7 to 3.2, −0.9 to 0.1, and −7.5 to −2.6, respectively (Fig. 4). All samples are supersaturated with respect to calcite and dolomite. There is a potential for precipitation of calcite and dolomite in the study area. The higher concentration of Cl^- correlates with the higher SIG and SIH values suggesting more dissolution of gypsum and halite in groundwater (Fig. 4).

Isotope composition of groundwater

Oxygen and hydrogen isotope ratios of the water samples relative to SMOW ($\delta^{18}O$ and $\delta^{2}H$) range from −0.06 to −4.65‰ and from −36 to 10.8‰, respectively (Table 1). Stable isotopic composition of samples is compared with eastern Mediterranean water line (EMWL) and global meteoric water line (GMWL) in Fig. 5. Most of the samples plot around the EMWL suggesting a Mediterranean meteoric source for groundwater. Comparison of isotope composition of the water samples shows enrichment from −3.6 and −7.9 in fresh waters (EC <5,000 μS/cm) to −2.7 and −5.1 in saline water (EC more than 5,000 μS/cm) for $\delta^{18}O$ and $\delta^{2}H$, respectively. High chloride content of the samples in saline water samples is in agreement with $\delta^{18}O$ enrichment (Table 1).

Salinization processes

Spatial distribution of EC and the chemical and isotopic composition of groundwater were used to differentiate the salinity sources. The high values of EC correspond to the areas characterized by shallow water table. In contrast, groundwater samples collected from the areas close to Abdan and Lombedan villages have low EC (Fig. 2). The variation of EC values along the groundwater flow paths is interesting and unusual. Although increasing of EC values

Table 1 Chemical and isotopic analysis of samples in the study area (EC: μS/cm; ions: mg/l; isotopes: permil)

No.	X	Y	T	pH	EC	HCO_3	Cl	SO_4	NO_3	Br	Ca	Mg	Na	K	Error%	$\delta^{18}O$	$\delta^{2}H$
PW1	572,821	3,108,665	26.2	8.1	4,160	109.8	886.3	1,306.9	2.5	–	400.8	206.6	327.8	13.3	2.2	–	–
PW2	572,876	3,108,467	26.2	7.9	3,520	122	567.2	1,374.1	3.3	–	324.6	170.2	263.7	11.3	4.3	–	–
PW3	572,779	3,109,307	26.2	7.7	2,420	146.4	248.2	1,306.9	1.4	–	276.6	130.1	185.1	12.5	5.3	–	–
PW4	572,991	3,109,377	26.1	7.5	2,840	152.6	248.2	1,576.3	1	3	330.7	154.4	190.8	16.4	5.4	−2.75	−5
PW5	573,401	3,108,159	26.2	7.7	2,900	128.1	283.6	1,542.7	1.6	–	357.7	178.1	199.3	15.6	0.7	–	–
PW6	572,523	3,109,545	26	7.8	2,130	103.7	248.2	801.1	1.9	–	200.4	87.5	158.6	8.2	2.1	–	–
PW7	573,233	3,109,255	25.9	7.8	1,790	146.4	134.7	685.9	2.2	–	180.4	97.2	97.9	9.8	2.4	–	–
PW8	573,143	3,109,128	26.3	7.7	2,560	91.5	248.2	1,340.5	2.2	–	292.6	136.1	158.6	15.2	4.7	–	–
PW9	596,043	3,089,990	26.4	7.7	3,670	146.4	602.7	1,306.9	3.4	–	300.6	167.7	295.7	14.5	5.1	–	–
PW10	596,819	3,086,954	26.3	7.8	2,830	134.2	336.8	1,340.5	1.1	–	216.4	184.8	225.5	15.2	4.4	–	–
PW11	596,490	3,087,124	26.1	7.6	3,920	146.4	467.9	1,896.7	3.5	5.2	376.8	216.4	320.9	17.2	3.8	−4.65	−5.9
PW13	596,938	3,087,500	26.1	7.9	2,850	152.6	496.3	1,003.3	8.9	–	260.5	160.4	179.8	15.2	4.1	–	–
PW14	597,038	3,087,619	26	7.9	3,270	122	531.8	1,205.6	3.2	–	258.5	155.6	275.4	15.2	5.4	–	–
PW15	597,183	3,087,907	26	7.8	3,870	140.3	354.5	1,138.3	3.6	–	276.6	144.6	194.7	15.2	5.3	–	–
PW17	595,472	3,087,921	26.1	7.7	4,860	170.9	797.6	1,863.1	2.7	–	430.9	243.1	391.7	17.2	4.1	–	–
PW18	595,247	3,087,657	26.3	7.6	6,440	183.1	1,293.9	2,284.8	4.6	9.4	501	486.2	535.7	21.5	1	−2.99	−7.7
PW19	595,389	3,087,581	26.3	7.6	5,130	170.9	797.6	2,031.7	2.3	–	521	352.5	407.6	18.4	3.9	–	–
PW20	595,024	3,087,537	26.4	7.9	8,220	256.3	1,825.7	2,992.7	1.7	–	701.4	498.4	703.5	34.4	4.6	–	–
PW22	595,702	3,088,371	27.1	6.03	5,050	195.3	992.6	1,601.3	–	15.1	420.8	334.3	497.5	17.98	3.1	–	–
PW23	597,581	3,089,021	26.4	8	2,410	140.3	283.6	1,138.3	3.9	–	336.7	136.1	180.9	14.5	5.9	–	–
PW24	597,965	3,089,211	26.4	7.8	3,100	122	319.1	1,407.8	5	3.1	356.7	94.8	227.4	15.2	2.4	−3.92	−6.8
PW25	596,988	3,089,123	26.1	7.9	2,380	152.6	258.8	1,138.3	1.3	–	236.5	198.1	155.9	10.9	2	–	–
PW26	596,310	3,089,583	26.1	7.9	4,480	177	723.2	2,048.5	1.6	–	390.8	328.2	375.7	16.4	2.5	–	–
PW27	574,381	3,107,738	26.1	7.8	2,600	122	308.4	1,205.6	2.6	–	266.5	154.4	177.5	10.6	5.2	–	–
PW28	573,551	3,108,409	26.1	7.7	2,900	140.3	375.8	1,273.3	2.7	–	362.7	111.8	179.8	14.5	5.4	–	–
PW29	573,733	3,108,648	26	7.9	2,210	146.4	237.5	936.1	1.7	–	324.6	46.2	123.9	9.8	4.4	–	–
PW30	572,704	3,108,403	26.1	8	3,730	122	514	1,610.4	2.6	–	428.9	128.8	310.4	11.7	4.1	–	–
PW31	572,335	3,108,283	26.4	7.9	2,290	109.8	237.5	1,138.3	3.6	–	270.5	99.7	131.7	7.8	5.8	–	–
PW32	572,580	3,108,204	26.4	7.9	2,590	134.2	319.1	1,143.1	2.4	–	258.5	107	212.9	7.8	5.2	–	–
PW33	572,720	3,107,882	26.4	8	2,020	122	212.7	952.9	3.2	–	230.5	99.7	119.3	7	5.6	–	–
PW34	572,534	3,107,932	26.4	7.9	2,500	91.5	283.6	1,239.2	4.9	–	314.6	107	156.3	7.8	5	–	–
PW35	572,269	3,107,577	26.4	7.6	2,050	122	322.6	1,475.5	3.4	–	398.8	119.1	183.2	5.1	5.2	–	–
PW36	572,434	3,107,386	26.3	7.8	3,200	122	390	1,390.9	5.1	–	376.8	122.8	199.8	7.8	5.3	–	–
PW37	572,432	3,107,591	26.2	7.8	2,700	97.6	276.5	1,390.9	4.7	–	378.8	103.3	157	7.8	4.7	–	–
PW38	572,547	3,107,756	26.1	7.9	2,530	128.1	230.4	1,374.1	3.3	–	336.7	125.2	150.1	7.4	2.7	–	–
PW39	572,930	3,107,527	26	7.7	3,000	122	372.2	1,273.3	5.4	–	318.6	147.1	199.8	8.6	4.6	–	–

Table 1 continued

No.	X	Y	T	pH	EC	HCO_3	Cl	SO_4	NO_3	Br	Ca	Mg	Na	K	Error%	$\delta^{18}O$	$\delta^{2}H$
PW40	572,780	3,107,462	26	7.9	3,190	128.1	425.4	1,357.3	5.9	–	400.8	115.5	204.4	8.2	4.8	–	–
PW41	573,166	3,107,323	26.5	7.8	3,650	109.8	567.2	1,559.5	6.2	–	416.8	142.2	295.7	9.8	5.3	–	–
PW42	573,155	3,107,482	26.3	7.7	2,880	134.2	390	1,138.3	3.7	–	284.6	127.6	189.7	8.6	5.4	–	–
PW44	573,444	3,107,224	26.5	7.7	3,660	128.1	620.4	1,306.9	4.5	–	360.7	156.8	247.8	9.8	5.4	–	–
PW45	573,690	3,106,882	26.4	7.6	6,160	122	1,595.3	1,374.1	4.6	–	541.1	340.3	407.6	5.1	3.8	–	–
PW46	573,927	3,106,270	26.4	7.9	7,630	164.8	2,038.4	1,779	5.2	–	581.2	425.4	615.7	15.2	5.7	–	–
PW47	582,589	3,100,688	26.4	7.9	6,910	213.6	1,577.5	1,981.2	–	–	651.3	261.3	599.6	27.4	4.9	–	–
PW48	578,592	3,103,114	26.1	7.8	6,130	152.6	1,400.3	1,779	4.7	–	491	267.4	567.6	16.4	3.8	–	–
PW50	595,385	3,090,395	26.1	7.8	6,220	152.6	1,293.9	2,065.3	6.6	–	871.7	127.6	519.6	20.3	5.3	–	–
PW52	573,108	3,108,480	26.2	7.7	2,620	128.1	354.5	1,087.9	2.8	–	290.6	116.7	155.9	12.5	5.8	–	–
PW53	572,811	3,109,591	26.4	7.5	2,640	189.2	265.9	1,242.1	0.2	–	292.6	127.6	160.5	13.3	4.2	–	–
OW7	574,528	3,107,637	26.3	8	2,400	122	390	834.8	1.2	3.5	190.4	133.7	163.9	11.7	3.5	−4.38	−7.8
OW8	576,332	3,105,392	26.3	7.8	4,900	128.1	939.4	1,390.9	2.6	7.2	380.8	316	375.7	16.4	0.1	−2.49	−5.2
OW5	575,326	3,104,523	26.1	7.6	4,480	152.6	709	2,065.3	1.1	–	390.8	352.5	375.7	18.4	5.9	–	–
OW36	574,217	3,099,951	26.2	8.5	14,170	85.4	3,545	4,510	1.4	26.9	541.1	771.8	1,879	44.2	4.1	−2.29	−1.2
OW37	575,505	3,095,760	26.2	8.3	11,250	73.2	2,836	3,073.9	1.9	–	491	443.7	1,639.2	37.1	7.5	–	–
OW38	580,436	3,094,466	26.2	8.6	30,200	54.9	9,305.6	5,648.3	0.2	57.9	901.8	765.8	5,019.4	38.3	4.6	–	–
OW39	586,334	3,092,541	26.2	8.6	35,100	79.3	12,407.5	4,603.2	0.9	–	992	790.1	6,697	52.8	1.4	–	–
OW15	595,098	3,090,176	26.3	7.5	6,790	140.3	1,418	2,149.8	1.9	13.6	601.2	407.2	471.8	21.5	4.7	−3.14	−6.5
OW29	592,052	3,091,721	26.3	8	12,610	299	4,714.9	0	10.5	–	130.3	285.6	2,161.1	87.6	4.7	–	–
OW30	591,797	3,093,851	26.3	7.3	7,980	225.8	2,038.4	1,879.9	3.1	15.4	591.2	364.7	711.5	28.2	3.5	–	–
OW31	587,557	3,097,748	26.3	8.1	6,030	73.2	1,772.5	2,116.7	0.4	–	697.4	273.5	703.5	29.3	4.6	–	–
OW32	584,502	3,098,518	26	7.5	7,770	183.1	1,772.5	1,900.5	1.1	–	551.1	303.9	783.5	32.5	5.7	–	–
OW33	584,651	3,098,864	26.2	7.3	7,710	195.3	1,719.3	1,947.6	0.8	–	591.2	224.9	767.6	29.3	4.8	–	–
OW34	582,848	3,100,934	26.2	7.2	7,540	183.1	1,701.6	1,863.1	0	–	591.2	255.3	687.6	39.1	4.5	–	–
OW35	580,358	3,100,573	26.2	7.6	13,120	61	3,545	3,161.3	1.1	–	861.7	498.4	1,543.5	28.2	5.5	–	–
OW11	578,273	3,103,334	26.3	8	5,590	225.8	1,364.8	1,273.3	0.3	–	324.6	249.2	551.8	29.3	4.8	–	–
Sp1	587,698	3,098,152	26.5	8.8	3,610	109.8	762.2	801.1	0.7	–	232.5	121.6	327.8	15.2	5.3	–	–
Sp2	585,278	3,101,618	26.5	7.8	3,860	207.5	673.6	1,104.7	0.3	7.4	302.6	142.2	311.7	16.4	4.6	–	–
SP5	583,943	3,101,430	26.2	7.4	6,010	170.9	1,240.8	1,779	0.5	–	565.1	212.7	503.7	24.2	0.4	–	–
Sp3	586,065	3,099,692	26.3	8.1	5,080	183.1	726.7	1,475.5	0.5	–	470.9	145.9	407.6	23.5	5.4	–	–
Sp4	598,252	3,090,652	26	8.1	2,850	201.4	301.3	1,425.1	0.4	2.9	336.7	151.9	171.7	16.4	9.4	−4.35	−19.7
Sea			26.4	8.4	51,100	189.2	21,270	3,373.6	0.6	150.7	561.1	1,507.2	9,262.2	100.1	2.8	−0.06	10.8
PW54	595,119	3,088,261	26.4	8	6,240	183.1	1,630.7	2,627.2	8.4	–	651.3	455.8	333.9	20.3	5.2	–	–
PW55	566,144	3,089,547	26.5	8	5,490	183.1	1,063.5	1,812.7	7	–	412.8	261.3	257.8	16.4	0.4	–	–
PW56	573,281	3,109,567	26.2	7.9	1,004	164.8	63.8	439.5	1.4	–	130.3	63.2	20.1	6.6	3.2	−3.2	−6.4

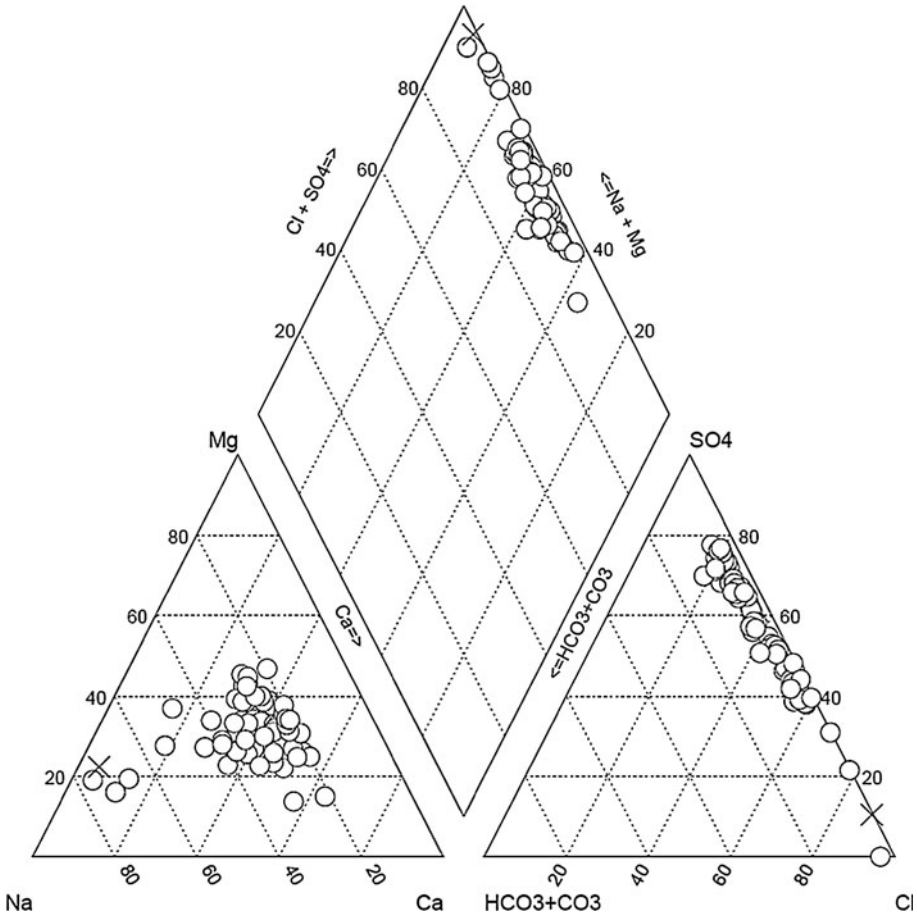

Fig. 3 Piper diagram for the water samples collected in Oct. 2008

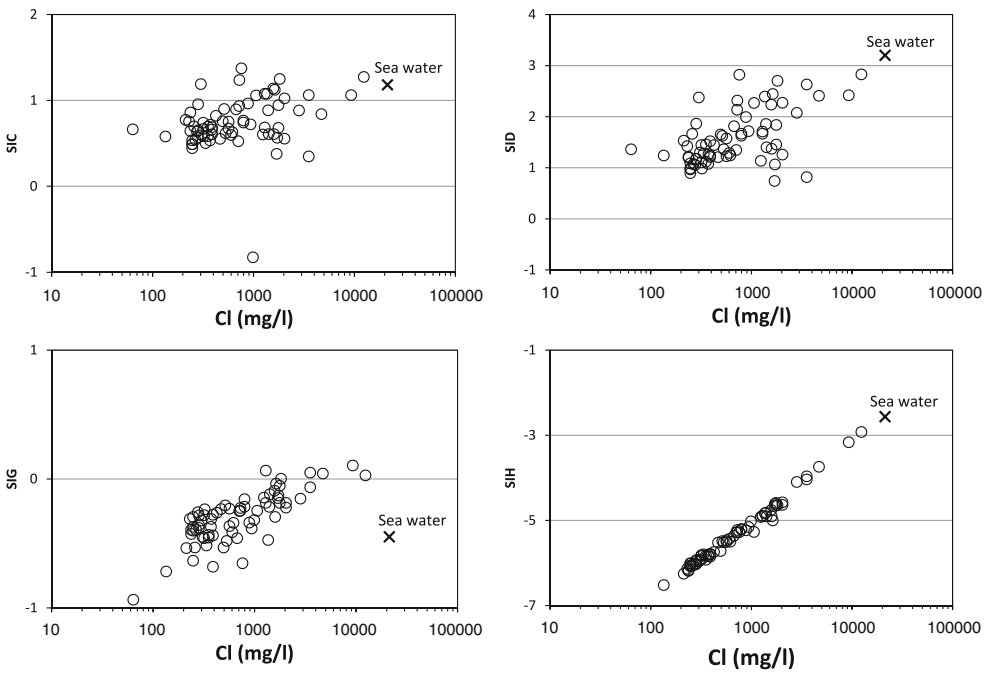

Fig. 4 Plot of saturation index with respect to common minerals versus concentration of Cl^-

as a representative of ions concentration along groundwater flow paths is an accepted general rule in groundwater studies, reverse trend can be caused by mixing of different waters. The spatial variation of other chemical variable, such as TDS, TH, and concentrations of Cl and Na follows the same pattern as EC.

Hydrogeologically, the recharged fresh water from Asmari limestone layers in the Namak Anticline may be mixed with saline groundwater which migrates from southern part of the plain (Fig. 2). In addition, groundwater quality may be affected by direct evaporation and perhaps sea water intrusion due to shallow groundwater depth and potential hydraulic gradient from sea toward the studied aquifer.

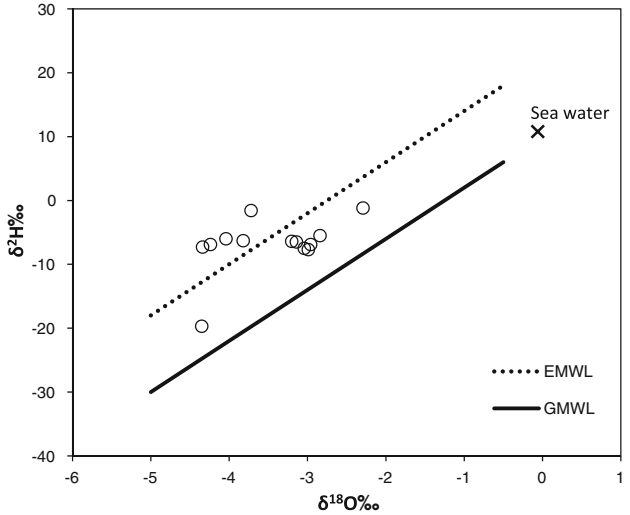

Fig. 5 Relationship of δ^2H and δ^{18}O in the studied samples with GMWL (Craig 1961) and EMWL (Gat 1981)

The relationship between Na^+, Ca^{2+}, Mg^{2+}, Br^-, NO_3^-, and HCO_3^- versus Cl^- can be used to demonstrate chemical variation in samples as a result of contribution of hydrochemical processes (Sami 1992; Vengosh and Rosenthal 1994; Faye et al. 2005). All samples are dispersed between two poles (end-members) and follow a linear trend almost in all composite diagrams (Fig. 6). Interestingly, this trend is not evident for NO_3^- (Fig. 6f), most probably due to the use of nitrogen fertilizer in the agricultural lands. The concentration of NO_3 was <10 mg/l in all samples and its maximum values were matched with spatial distribution of agricultural activities (Sharifzade 2009). The concentration of HCO_3^- did not show an increasing trend with increasing the concentration of Cl^- (Fig. 6e). HCO_3^- was mainly driven by dissolution of carbonate minerals such as calcite and dolomite in the presence of dissolved CO_2 in groundwater. Consequently, the concentration of HCO_3^- is

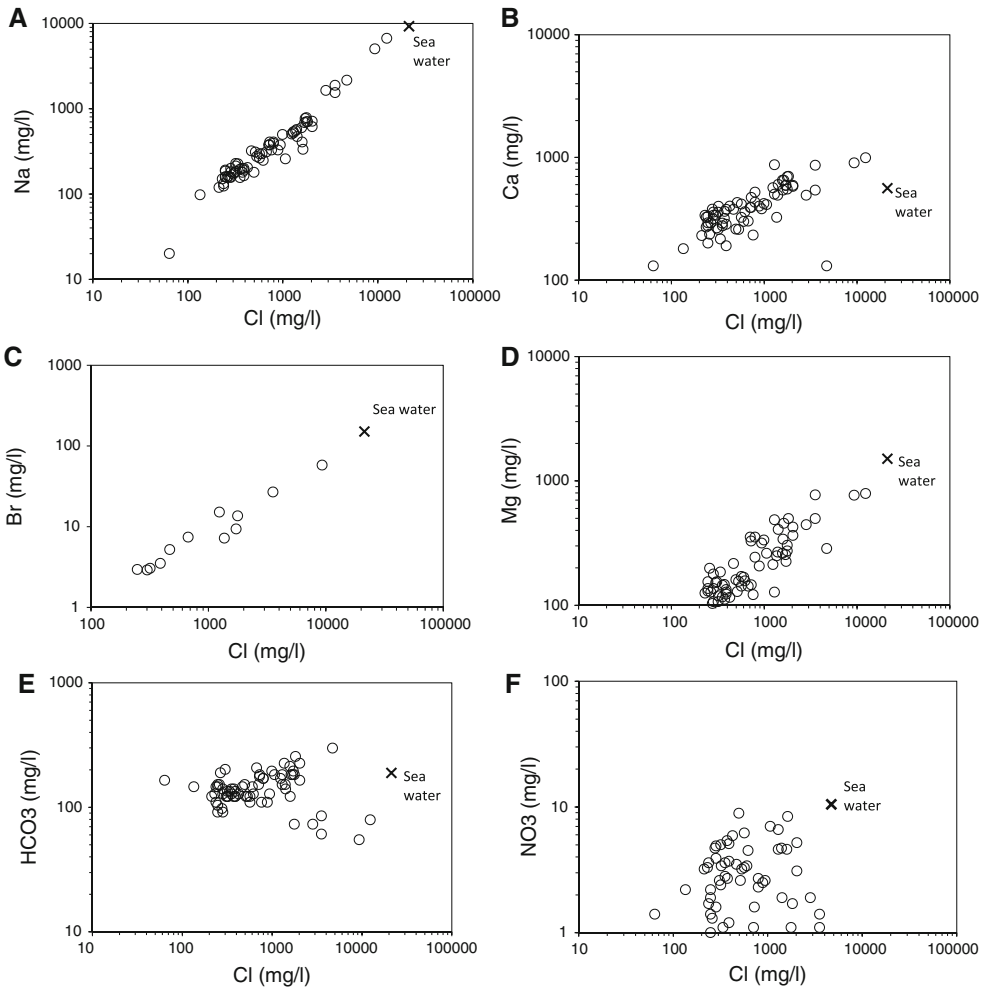

Fig. 6 Composite diagram of chemical constituents versus Cl

nearly constant in fresh water samples and slightly decreased in saline water samples as a result of precipitation of carbonate minerals during evaporation.

The concentration of Na^+ ranges from minimum 20 mg/l to maximum 9,262 mg/l in saline water samples. The trend of Na^+ and Cl^- does not follow a 1:1 trend line, suggesting the effect of additional chemical processes other than dissolution of halite (Fig. 6a). The concentration of Ca^{2+}, Mg^{2+}, and Br^- increases in different rates with increasing Cl^- concentration (Fig. 6b–d). These behaviors may be the result of different concentrations of these ions of the end-members (i.e., fresh and saline water) and the effect of other chemical processes other than mixing. The concentration of Br^- in the study area ranges from 2.9 to 150.73 mg l^{-1}. Concentration of Br^- may be enriched due to evaporation and/or seawater intrusion (Fig. 6c). There are several indications of mixing between two end-members as fresh and saline sources: (1) EC values reduce from more than 35,000 to less than 2,000 μS/cm along flow lines (Fig. 2); (2) a linear plot of the samples on Piper diagram (Fig. 3); (3) the linear trend between two end-members in plots of major ions and Br^- versus Cl^- (Fig. 6); and (4) the isotopic composition of the water samples in comparison with isotopic composition of sea water and freshwater samples (Fig. 5). In order to find out the percentage of saline water (f_s) in each sample, estimation is made based on the linear mixture of fresh and saline water end-members as follows:

$$f_s = (Cl_{sample} - Cl_f)/(Cl_s - Cl_f) \quad (2)$$

where Cl_{sample}, Cl_f, and Cl_S are concentrations of Cl in mixed sample, fresh water, and saline water, respectively. According to groundwater flow pattern (Fig. 2), sample OW38 in western part of the area close to Derang Anticline in Fig. 1 and seawater are considered as saline end-members. Sample PW54 with the lowest EC is considered as representative of fresh end-member. Solving Eq. 2 for mixing ratio (f_s) by assuming seawater and sample OW38 as saline end-members show that the maximum mixing ratios of saline water are 8 and 15%, respectively. Chloride was assumed as a conservative species during the mixing processes. However, concentration of Cl^- could be modified due to evaporation and environmental processes, i.e., irrigation return flow.

Generally, high concentration of Cl^- is correlated with high concentration of major ions, suggesting a linear mixing between two chemically distinct end groups (Fig. 6). However, the linear simple mixing between two end groups (i.e., fresh and saline water) may be disturbed by several known hydrochemical processes such as dissolution precipitation of minerals, evaporation, and cation exchange. The major hydrochemical processes are discussed in the following sections.

Water–rock interaction

The lithology of the alluvial aquifer is the result of erosion process on surrounding formations which mainly consist of limestone, dolomite, gypsum, marl, sandstone, conglomerate, and partly halite. Dissolution of these minerals could release some ions to groundwater. Therefore, the HCO_3^-, Ca^{2+} and Mg^{2+} may be mainly derived by water–rock interaction in the study area. Comparison of molar content of $(Ca^{2+} + Mg^{2+})$ with $(2HCO_3^- + SO_4^{2-})$ is used to evaluate the contribution of dominant rock-forming minerals including calcite, dolomite, and gypsum (Fig. 7). It is seen in Fig. 7 that although most of the samples plot around the 1:1 trend, deviation of data from the 1:1 line suggesting a process such as cation exchange which could modify the concentration of cations in some parts of the study area (Sami 1992).

Dissolution of halite can provide a part of Na^+ concentration in groundwater which is equal to Cl^- molar concentration. The molar content of $(Ca^{2+} + Mg^{2+} - SO_4^{2-} - 2HCO_3^-)$ versus $(Na^+ - Cl^-)$ is used to estimate the concentration of Na^+, Ca^{2+}, and Mg^{2+} resulted from the dissolution of halite, dolomite, calcite, and gypsum (Fig. 8). Assuming that all Na, Ca, and Mg are released from dissolution of halite, calcite, dolomite, and gypsum as a geologic source, the values of $(Ca^{2+} + Mg^{2+} - SO_4^{2-} - 2HCO_3^-)$ and $(Na^+ - Cl^-)$ reach a minimum value close to zero. Figure 8 shows a deviation from geologic source for major cations. Small depletion of Na^+ in fresh water samples and enrichment of Ca^{2+} and Mg^{2+} in saline water samples could be caused by cation

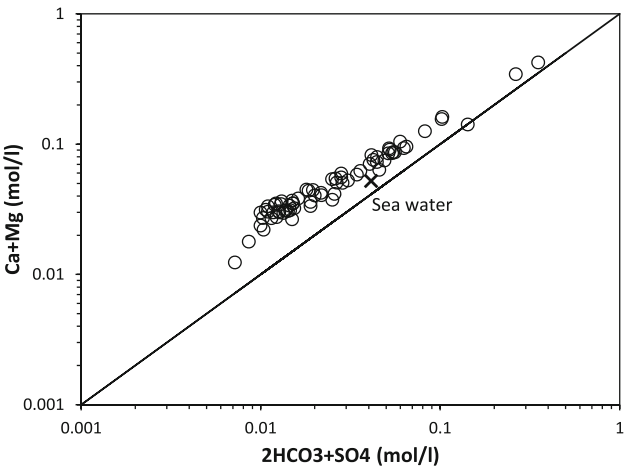

Fig. 7 Scatter plot of Ca + Mg versus $2HCO_3 + SO_4$ of groundwater samples

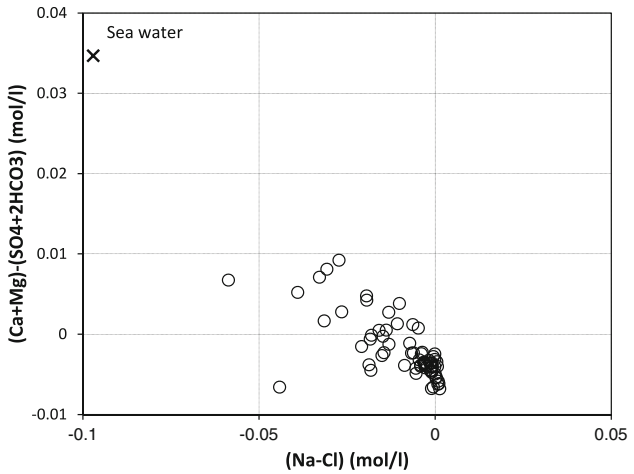

Fig. 8 Plot of (Ca + Mg) − (SO_4 + 2HCO_3) versus (Na–Cl) molar ratio

exchange process (Sami 1992; Kim et al. 2003; Wen et al. 2005).

The cation exchange often occurs in coastal aquifers during intrusion or freshening processes (Appelo and Postma 2005). The general cation exchange reactions are

$$2Na^{+}(K^{+}) + Ca^{2+} - X = 2Na^{+}(K^{+}) - X + Ca^{2+} \quad (3)$$

$$2Na^{+}(K^{+}) + Mg^{2+} - X = 2Na^{+}(K^{+}) - X + Mg^{2+} \quad (4)$$

where X represents cation exchange sites in aquifer materials (Appelo and Postma 2005) and ions in molar concentration. The reverse reaction occurs when Ca-rich fresh water flows to saline porous media. In the presence of cation exchange processes, the molar content of (Na + K) and (Ca + Mg) in samples could be deviated from line 2:1 as suggested by Sami (1992). Enrichment of Ca + Mg in the water samples could occur by cation exchange where saline water flows to the aquifer and potentially sodium is absorbed and calcium and/or magnesium are released (Fig. 9). However, samples with high EC (i.e., saline water samples) plot above the 2:1 line because of being not affected by cation exchange in the beginning of the groundwater flow path. Conceptually, saline water through migration toward coastal aquifer not only mixed with fresh water but also modified by cation exchange processes.

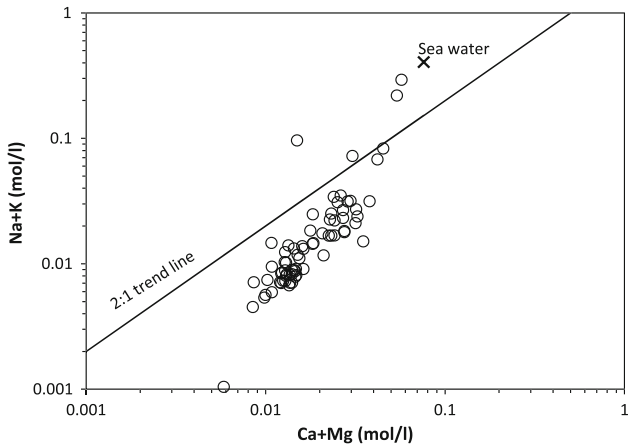

Fig. 9 Plot of (Na + K) versus (Ca + Mg) molar ratio

Evaporation

The aquifer in the study area is unconfined and the water table is not deep in some parts. The evaporation from groundwater table is mainly related to groundwater depth and soil properties of vadose zone. The water table depth in the saline water samples varies between 3 and 10 m which are shallow enough for direct evaporation. The effect of evaporation is intensified by high capillary fringe due to fine-grained sediment in these parts of the plain. However, the water table depth in the northern margin of the plain (belongs to fresh water samples) is more than 30 m which is too deep for any direct evaporation. Pan evaporation data shows a value of 2,600 mm/year in average for the area

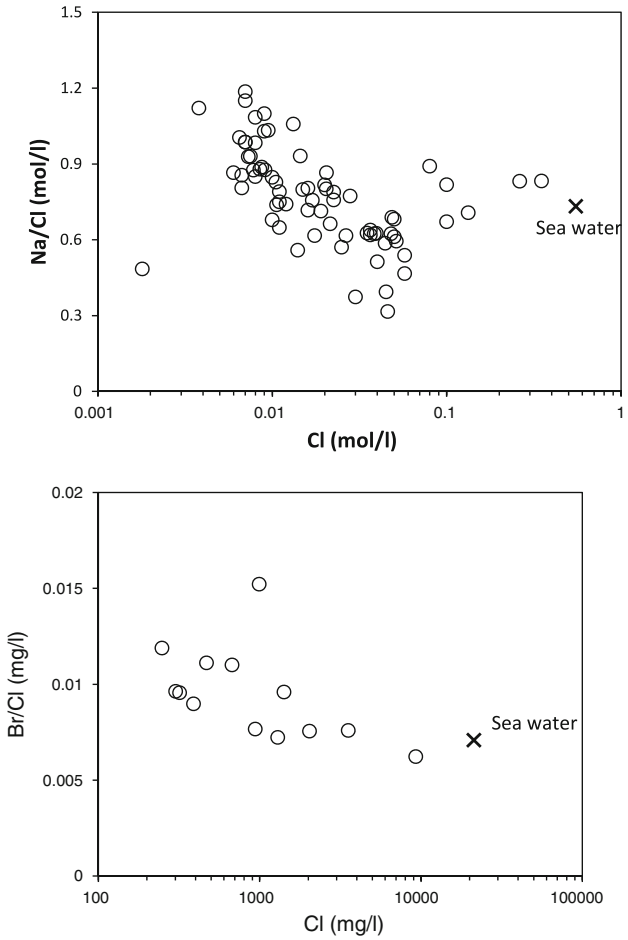

Fig. 10 Plot of Na/Cl and Br/Cl ratio versus concentration of Cl in the study area

(Sharifzade 2009). Evaporation from groundwater table could be evidenced according to two chemical indicators: (1) enrichment in stable isotopic composition of the saline water samples in comparison with the fresh water samples (Fig. 5) and (2) low Na^+/Cl^- and Br^-/Cl^- ratios for the samples mainly in the saline water samples. Generally, Br^- and Cl^- are conservative and the Br^-/Cl^- ratio in waters with certain sources (e.g., fresh water and sea water) is constant. Values about 0.0015 for Br^-/Cl^- ratio could be considered as the effect of seawater intrusion (Vengosh et al. 1999). The samples in group 2 show Na^+/Cl^- ratios <0.8 (Fig. 10a) and Br^-/Cl^- ratios <0.01 (Fig. 10b). These low values could be considered as indicators of evaporation from water table (Vengosh and Rosenthal 1994).

Irrigation return flow

Groundwater irrigates vast fields of tomato in western and eastern parts of the study area close to Abdan and Lombedan villages (Fig. 1). Therefore, groundwater is intensively exploited by production wells in these two specific locations. A part of the irrigation return flow infiltrates into water table flushing the pesticides, nitrogen fertilizers, and the salts deposited in top soil into aquifer. The anomaly in concentration of NO_3^- observed in the area is caused by contaminated irrigation return flow (Table 1; Fig. 6f).

Conclusions

The results of this study show that the migration of saline water toward the fresh water has an important role in degradation of groundwater quality in the study area. This condition was aggravated by over-pumping of groundwater and modification of natural groundwater flow pattern in recent years. The mineralization of groundwater (e.g., EC) ranges from 1,000 to more than 50,000 $\mu S\ cm^{-1}$. The spatial distribution of EC values in the study area reveals combinations of several geochemical processes that are responsible for chemical composition of groundwater in the studied plain. Results emphasizes that the mixing of saline water and fresh water is the main contribution to the groundwater quality degradation. It must be noticed that the expected chemical composition of mixed samples may be modified in the presence of several chemical processes such as cation exchange, dissolution and precipitation of minerals, evaporation, and so on. It seems that the reduction of pumping rate could help improve groundwater quality. As a final conclusion, understanding the processes and factors that control chemical composition of groundwater plays the main role in the management of coastal aquifers.

Acknowledgments This research was partly supported by Bousheher Water Authority (Water Resources Management Organization of Iran). The authors thank The Research Counsel of Shiraz University for permanent support of this research and the Hydrogeochemistry Lab of the Earth Sciences Department of the Shiraz University. The authors would like to thank Dr. J. Bruthans from the Faculty of Science, Department of Hydrogeology, Charles University, Prague, Czech Republic, and Dr. J. Barker from the Earth and Environmental Sciences, University of Waterloo, Canada, for isotope and Br analysis, respectively. The constructive comments of two anonymous reviewers on first version of the manuscript were appreciated.

References

Alavi M (2004) Regional stratigraphy of the Zagros Fold-Thrust Belt of Iran and its pro-foreland evolution. Am J Sci 304: 1–20

Appelo T, Postma D (2005) Geochemistry, groundwater, and pollution. A.A. Balkema Publishers, Leiden, p 649

Backalowicz M (1994) Water geochemistry: water quality and dynamics. In: Groundwater ecology. Academic press, New York, pp 97–127

Bousheher water authority (2000) Geophysical study of Abdan-Dayer Plain, p 158 (in Farsi)

Bousheher water authority (2005) Annual report on hydrogeology of Abdan-Dayer Plain, p 52 (in Farsi)

Craig H (1961) Isotope variations in meteoric water. Science 133:1702–1703

Drever JI (1982) The geochemistry of natural waters. Prentice Hall, Englewood Cliffs, p 387

Faye S, Maloszewski P, Stichler W, Trimborn P, Faye SC, Gaye CB (2005) Groundwater salinization in the Saloum (Senegal) delta aquifer: minor elements and isotopic indicators. Sci Total Environ 343:243–259

Gat JR (1981) Groundwater. In: Gat JR, Gonfiantini R (eds) Stable isotope hydrology. International Atomic Energy Agency, Vienna, pp 223–400

Hem lD (1985) Study and interpretation of the chemical characteristics of natural water. USGS Water Supply Pap 2254:264

Kim Y, Lee KS, Koh DC, Lee DH, Lee SG, Park WB, Koh GW, Woo NC (2003) Hydrogeochemical and isotopic evidence of groundwater salinization in a coastal aquifer: a case study in Jeju volcanic island, Korea. J Hydrol 270:282–294

Kouzana L, Mammou AB, Felfoul MS (2009) Seawater intrusion and associated processes: case of the Korba Aquifer (Cap-Bon, Tunisia). CR Geosci 341:21–35

Parkhurst DL, Appelo CAJ (1999) User's guide to PHREEQC (version2): a computer program for speciation, batch reaction, one-dimensional transport and inverse geochemical calculations. Water resources investigations, report 95-4259, US Geological Survey, Denver, Colorado, p 312

Petals CP, Diamantis IB (1999) Origin and distribution of saline groundwaters in the upper Miocene aquifer system, coastal Rhodope area, northeastern Greece. Hydrogeol J 7:305–316

Post VEA (2005) Fresh and Saline groundwater interaction in coastal aquifers: is our technology ready for the problems ahead? Hydrogeology J 13:120–123

Richter BC, Kreitler CW (1993) Geochemical techniques for identifying sources of ground-water salinization. CRC Press, Boca Raton

Sami K (1992) Recharge mechanisms and geochemical processes in a semi-arid sedimentary, Eastern Cape, South Africa. J Hydrol 139:27–48

Sharifzade B (2009) The study of groundwater quality degradation in a coastal aquifer using hydrochemical parameters: Abdan-Dayer Plain, M.Sc thesis, Department of Earth sciences, Shiraz university, Shiraz, Iran, p 229 (in Farsi)

Stocklin J (1968) Structural history and tectonics of Iran, A review. AAPG Bull 52(7):1229–1258

Vengosh A, Rosenthal E (1994) Saline groundwater in Israel: its bearing on the water crisis in the country. J Hydrol 156:389–430

Vengosh A, Spivack AJ, Artzi Y, Ayalon A (1999) Geochemical and boron, strontium isotopic constrains on the origin of the salinity in groundwater from the Mediterranean coast of Israel. Water Resour Res 35:1877–1894

Wen X, Wu Y, Su J, Zhang Y, Liu F (2005) Hydrochemical characteristics and salinity of groundwater in the Ejina Basin, Northwestern China. Environ Geol 48:665–675

Zammouri M, Siegfried T, El-Fahem T, Kriaa S, Kinzelbach W (2007) Salinization of groundwater in the Nefzawa oases region, Tunisia: results of a regional scale hydrogeologic approach. Hydrogeology J 15:1357–1375